ACS OMEGA

http://pubs.acs.org/journal/acsodf

Article

Raman, WAXS, and Solid-State NMR Characterizations of Regenerated Silk Fibroin Using Lanthanide Ions as Chaotropic Agents

Giorgio Rizzo, Valentina Petrelli, Teresa Sibillano, Liberato De Caro, Maria Michela Giangregorio, Marco Lo Presti, Fiorenzo G. Omenetto, Cinzia Giannini,* Piero Mastrorilli,* and Gianluca M. Farinola*

Cite This: *ACS Omega* 2023, 8, 24165−24175

Read Online

ABSTRACT: *Bombyx mori* silk fibroin (SF) has been reported as a convenient natural material for regenerative medicine, optoelectronics, and many other technological applications. SF owes its unique features to the hierarchical organization of the fibers. Many efforts have been made to set up protocols for dissolution since many applications of SF are based on regenerated solutions and fibers, but chaotropic conditions required to disassemble the packing of the polymer afford solutions with poor crystalline behavior. Our previous research has disclosed a dissolution and regeneration process of highly crystalline fibers involving lanthanide ions as chaotropic agents, demonstrating that each lanthanide has its own unique interaction with SF. Herein, we report elucidation of the structure of Ln−SF fibers by the combined use of Raman spectroscopy, wide-angle X-ray scattering (WAXS), and solid-state NMR techniques. Raman spectra confirmed the coordination of metal ions to SF, WAXS results highlighted the crystalline content of fibers, and solid-state NMR enabled the assessment of different ratios of secondary structures in the protein.

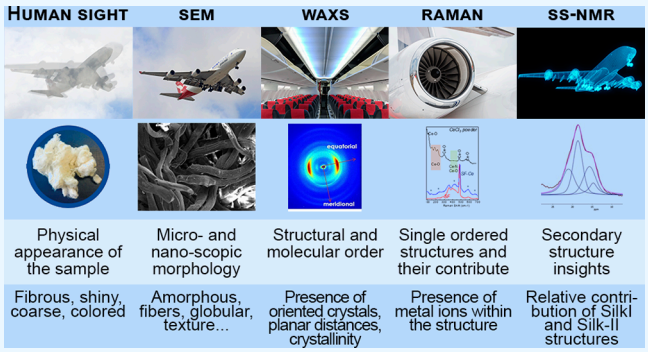

1. INTRODUCTION

Silks are a wide class of proteins with some unique features. They are high molecular weight proteins, possess considerable stiffness and flexibility, and are mainly composed of simple amino acids such as L-glycine and L-alanine. High concentration of these amino acids makes silks a class of chemically and thermally stable proteins since repeated regular sequences of these amino acids with few others generate highly ordered and packed crystals inside the biopolymer. Although silks are produced by several insects in their larval state for the metamorphosis and some adult animals, silk massive production is mostly limited to spiders and especially silkworms.[1,2] *Bombyx mori* silk fibroin (SF) is the protein part of the raw cocoon and its secondary structures comprise mostly β-sheet domains and amorphous regions, although a small number of helices and β-turns are also detected. More specifically, SF has two main assemblies, namely Silk I and Silk II, which are referred to before spinning and spun fibrous SF, respectively.[3] Silk I is rich in amorphous and highly flexible structures such as helices and coils, while Silk II, rich in β-sheets, is responsible for the resistance and stiffness of the biopolymer, enclosing the crystalline phases of the protein. Actually, Silk I is the metastable and still soluble processable form of SF before it is spun outside the living organism. SF has a very complex structure, as reported in Figure 1, consisting of two big bundles called brines, covered with sericin, a serine-rich gluey substance that contributes to creating the highly closed assembly of fibers in cocoons.[4,5] Each brine is then composed of highly packed fibrils, further divided into microfibrils, nanofibrils, and finally the single polypeptide filament.[6]

Fiber complexity extends also in the supramolecular arrangement of single polypeptide chains. As shown in Figure 1, the monomer, SF megamer, weighs 2.3 MDa, and it is composed of heavy fibroin (HF, 350 kDa, 92% w/w), light fibroin (LF, 26 kDa, 7% w/w), and fibrohexamerin (P-25, 30 kDa, 1% w/w), in a unique assembly of a 6:6:1 protein molar ratio, creating a hexagon-shaped cylinder.[7,8] L-Glycine, L-alanine, and L-serine constitute 45.9, 30.3, and 12% of the total

Received: November 6, 2022
Accepted: April 12, 2023
Published: June 28, 2023

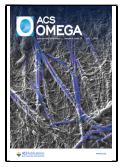

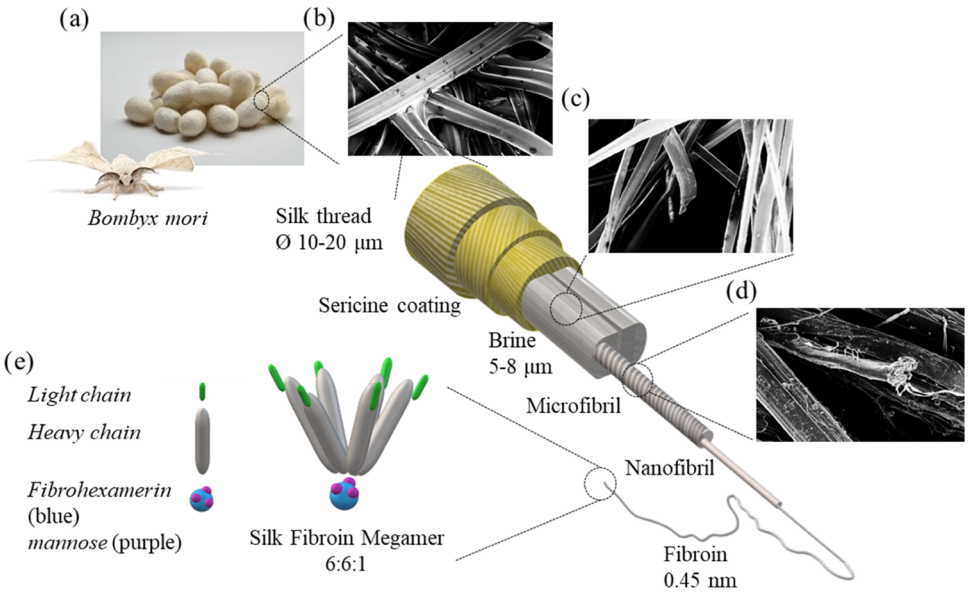

Figure 1. Overview of an SF thread. (a) *B. mori* cocoons, with a moth inset. (b) Scanning electron microscopy SEM image of the cocoons, highlighting the double bundle structure enveloped in the sericin gluey cement. (c) SF polypeptide after a degumming step in which sericin coatings are removed. (d) SEM image of a microfibril, showing a cross section in which nanofibrils can be observed. (e) SF megamer schematic structure showing the hexagonal shape arrangement of the three components of SF. Each light chain (in green) is bound via a sulfide bond to a heavy chain (gray) and together they are further combined in a hexagonal shape held together by the fibrohexamerin (in blue) via noncovalent bonding between the heavy chain and the mannose units (in purple), constituting the SF megamer (6 light chains, 6 heavy chains, and 1 fibrohexamerin, 6:6:1).

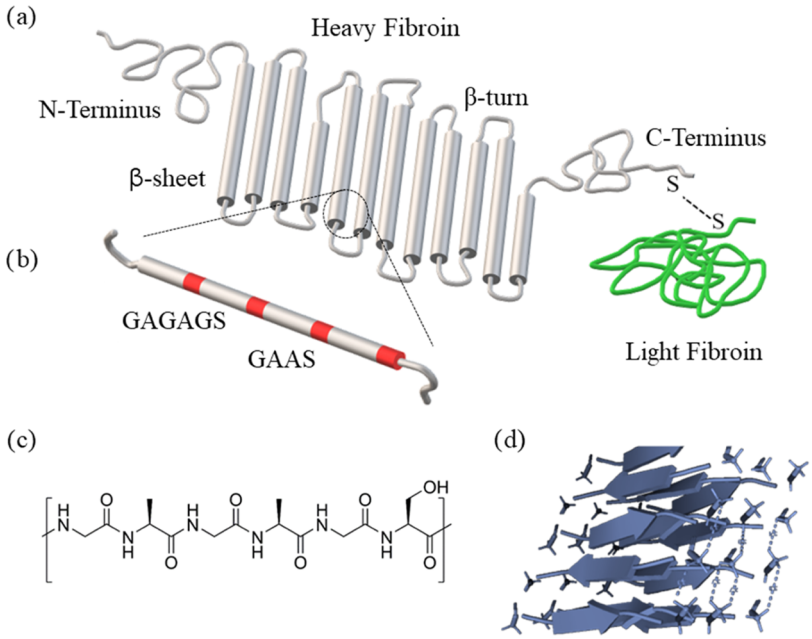

Figure 2. Structure and chemical composition of heavy fibroin. (a) Protein secondary structure. (b) Amino acidic sequence of one of the hydrophobic parts of the protein. (c) Chemical structure of the hexapeptide GAGAGS in SF. (d) β-sheets that rearrange in the closely packed β-crystals, with an antiparallel alternating fashion.

heavy fibroin weight, respectively.[9] Two hexapeptides GAGAGS and GAGAGY compose about 70% of the protein. Figure 2 shows the schematized structure of heavy fibroin.

The protein can be dissolved in concentrated aqueous solutions of inorganic acids (H_3PO_4, H_2SO_4, HCl)[10−14] and in saturated solutions of salts such as LiBr,[15] $CaCl_2$,[16] $Ca(NO_3)_2$,[17] or Schweitzer reagent ($CuSO_4$ in NH_3).[18] Other conditions for dissolution are the use of hexafluoroisopropanol (HFIP) and hexafluoroacetone (HFA)[19,20] and the ionic liquid *N*-methylmorpholine *N*-oxide NMMO.[21]

Our previous investigations led to the discovery of a new dissolution and fiber regeneration procedure involving $CeCl_3 \cdot 7H_2O$.[22] Starting from this evidence, a systematic investigation of all of the lanthanide ions as chaotropic agents was performed.[23] The results of this study showed the unique ability of each lanthanide ion to dissolve SF and to regenerate it with different degrees of crystallinity depending on the metal

https://doi.org/10.1021/acsomega.2c07149
ACS Omega 2023, 8, 24165−24175

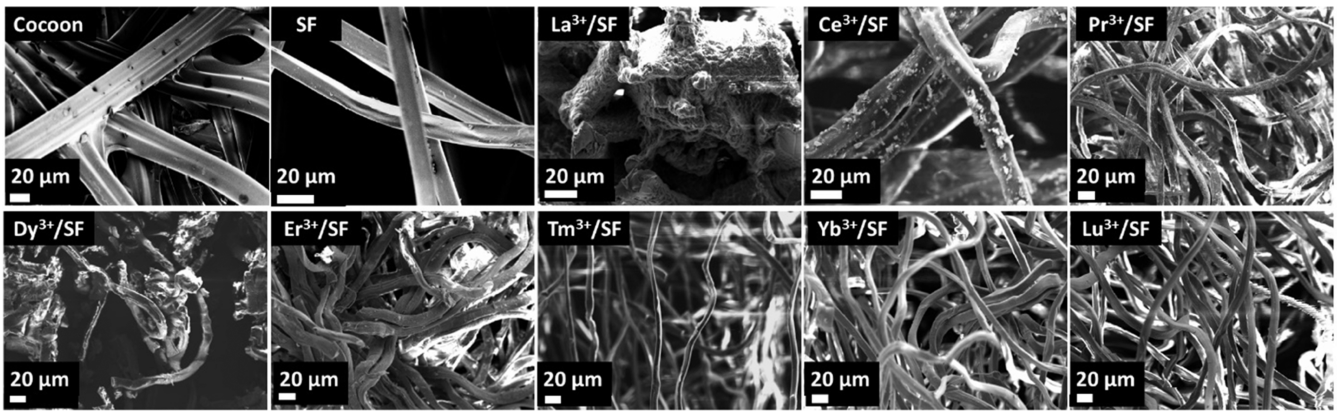

Figure 3. SEM images of Ln^{3+}/SF fibers. For comparison, SEM images of natural *B. mori* cocoon and degummed SF are also reported. The scale bar refers to 20 μm. Images adapted in part from ref 23. Copyright 2021, owner Rizzo, Lo Presti, Giannini, Sibillano, Milella, Guidetti, Musio, Omenetto and Farinola (Frontiers in Bioengineering and Biotechnology).

used.[24−28] However, the fine molecular architecture of the Ln−SF fibers, in terms of the exact amount of the secondary structure and of crystalline content for each sample, remained not fully elucidated. In this study, a multitechnique characterization of the SF regenerated using lanthanide ions as chaotropic agents is presented based on Raman, WAXS, and solid-state NMR.

Our investigation started from previously acquired data, such as (SEM) images and preliminary WAXS analyses, with the aim of obtaining a multiscale characterization of regenerated SF samples.[23] These results were properly adapted and further discussed here in order to create a comprehensive view of all of the information obtained for a deep structural characterization of a new material.

Precisely, Raman analyses gave information about the presence of chelated metal ions within the biopolymer structures, WAXS shed light on the crystalline nature of all regenerated Ln−SF materials, and solid-state NMR showed the single structural contributions in all samples, thus allowing to distinguish between Silk I-like and Silk II structural motifs.

2. MATERIALS AND METHODS

2.1. General Information. All of the hydrated lanthanide chlorides ($LaCl_3{\cdot}7H_2O$, $CeCl_3{\cdot}7H_2O$, $PrCl_3{\cdot}7H_2O$, $DyCl_3{\cdot}6H_2O$, $ErCl_3{\cdot}6H_2O$, $TmCl_3{\cdot}6H_2O$, $YbCl_3{\cdot}6H_2O$, $LuCl_3{\cdot}6H_2O$) were purchased from NOVA ELEMENTS SAS (Palermo, Italy). All other chemicals and solvents were purchased from Sigma Aldrich. All compounds were used without any further purification.

2.2. SF Degumming. SF was obtained by a standard procedure starting from *B. mori* raw cocoon acquired from Tajima Shoji (Japan).[29] Briefly, 5.0 g of raw cocoons was shredded into ∼1 cm pieces and boiled in a 2 L aqueous solution of 0.02 M Na_2CO_3 for 30 min to discharge the external sericin coating. In the following, the pure protein part (∼3.5 g, 75% of the whole cocoon weight) was rinsed several times in fresh distilled water to remove sericin and the excess salt used. SF was dried under ambient temperature for 48 h before proceeding with its dissolution and regeneration with lanthanides.

2.3. SF Dissolution and Fiber Regeneration with $LnCl_3{\cdot}nH_2O$. According to the new dissolution procedure discovered in our laboratories based on the substitution of $CaCl_2$ in Ajisawa's protocol[16] with hydrated lanthanide chlorides, Ln^{3+}/SF samples were obtained.[22,23] A hydro-alcoholic solution of $LnCl_3{\cdot}nH_2O$ was prepared to maintain a molar ratio of 1:8:2 between the lanthanide salt (9.51 mmol, 3.532 g of $LaCl_3{\cdot}7H_2O$; 3.544 g of $CeCl_3{\cdot}7H_2O$; 3.554 g of $PrCl_3{\cdot}7H_2O$; 3.585 g of $DyCl_3{\cdot}6H_2O$; 3.630 g of $ErCl_3{\cdot}6H_2O$; 3.650 g of $TmCl_3{\cdot}6H_2O$; 3.768 g of $YbCl_3{\cdot}6H_2O$; 3.708 g of $LuCl_3{\cdot}6H_2O$) water (1.38 g), and ethanol (0.88 g), respectively. After slight heating to promote complete dissolution of the salts, 0.250 g of degummed SF was submerged and dissolved at 60 °C for 4 h. The viscous SF solutions were then inserted in a dialysis cassette using a regenerated cellulose dialysis membrane (MWCO 12.400 g mol^{-1}) against bidistilled water to remove the lanthanide salts and hence promote fibrous thread precipitation. The purification required three water batches. After that, the fibers were quantitatively recovered and allowed to dry under ambient temperature for 48 h before analyzing them. Aqueous solutions of dialyzed samples were collected and treated with a Na_2CO_3 solution to recover the lanthanides as insoluble carbonates. They were filtered and redissolved in a minimum amount of a 3 N HCl aqueous solution and allowed to crystallize in the form of $LnCl_3{\cdot}nH_2O$ salts.

2.4. Solid-State NMR Analyses. Solid-state NMR analyses were performed on a Bruker Avance I 400 spectrometer (operating at a frequency of 100.6 MHz for ^{13}C and 40.3 MHz for ^{15}N) using a 4.0 mm HX MAS probe at 298 K. Samples were packed in 4 mm zirconia rotors and spun at 7 kHz (^{13}C) or 10 kHz (^{15}N) under airflow. $^{1}H-^{13}C$ CP/MAS NMR experiments were acquired using a 3.25 μs proton $\pi/2$ pulse length, a ν_{CP} of 55.0 kHz, a contact time of 1.0 ms, a ν_{dec} of 76.9 kHz, and a recycle delay of 4.0 s. $^{1}H-^{15}N$ CP/MAS NMR experiments were acquired using a contact time of 2.5 ms and a recycle delay of 6.0 s. A two-pulse phase-modulation (TPPM) decoupling scheme was used for the ^{1}H decoupling. Chemical shifts for ^{13}C were referenced to $SiMe_4$ (0 ppm) by using the methylene signal of adamantane (δ 38.48) as a secondary reference, while ^{15}N chemical shifts were referenced to liquid NH_3 (0 ppm) using the ^{15}N-glycine signal (33.4 ppm) as a secondary reference.

Lineshape analysis and the fractions of various components of the Ala Cβ peaks were determined using a peak deconvolution analysis with software MestReNova 11.0 (MestReNova Research SL, Santiago de Compostela, Spain).

https://doi.org/10.1021/acsomega.2c07149
ACS Omega 2023, 8, 24165−24175

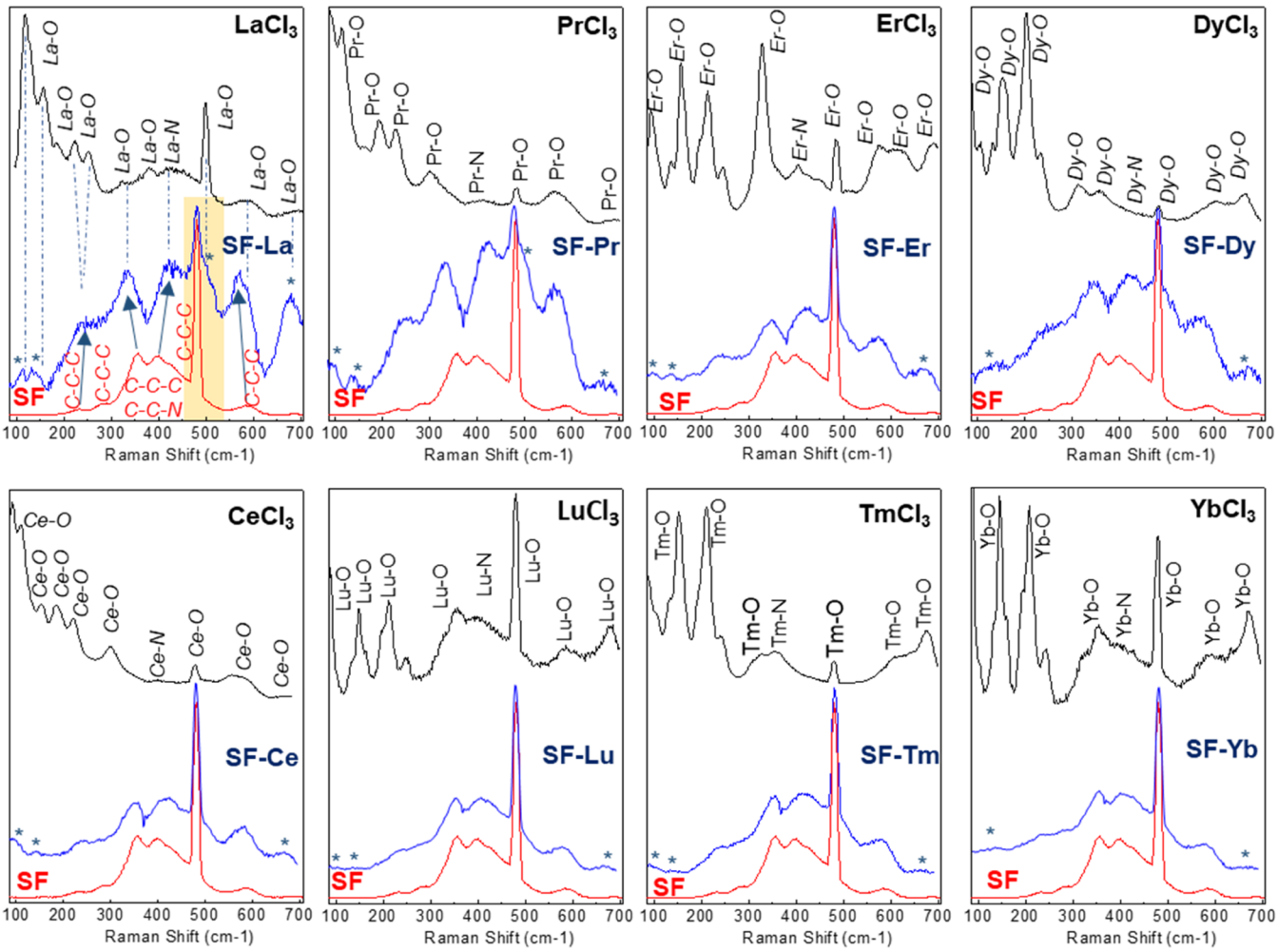

Figure 4. Raman spectra of different Ln-doped silk fibers (blue line, SF−Ln) compared with degummed silk fibroin (red line, SF) and the corresponding hydrated $LnCl_3$ salts (black line). (*) indicates vibrational bands in spectra of Ln-doped SF due to the formation of bonds between Ln and O and N (Ln−O, Ln−N). Dotted blue lines in the spectrum of SF−La highlight the correspondence between the vibrational bands due to La−O and La−N bonds in the Raman spectrum of hydrated $LaCl_3$ salt and bands in the spectrum of SF−La. Blue arrows indicate the shift of some peaks in the Raman spectrum of degummed SF after La doping. The orange area highlights the change in the symmetry of the peak at ∼480 cm^{-1} after doping. The Ln−N vibrational band has been indicated in the spectra of salts also when it is not visible in order to investigate the possibility of bonds between Ln and N in SF.

2.5. WAXS Analyses. WAXS experiments were performed at the X-ray Micro Imaging Laboratory (XMI-LAB) of the Institute of Crystallography of CNR-Bari[30−32] The laboratory is equipped with a Fr-E+ SuperBright rotating copper anode microsource (λ = 0.154 nm, 2475 W) coupled through a focusing multilayer optics confocal max-flux to a SAXS/WAXS three pinhole camera equipped for X-ray scanning microscopy. An image plate (IP) detector (250 × 160 mm^2, with 100 μm effective pixel size), with an offline RAXIA reader, was used to collect WAXS data. The spot size at the sample position was around 200 μm. The detector was placed at around 10 cm from the samples, giving access to a range of scattering vector moduli ($q = 4\pi \sin \vartheta/\lambda$) from 0.3 to around 3.5 $Å^{-1}$, which corresponds to a 1.8−25 Å d-spacing range.

2.6. Raman Analyses. Raman spectra were collected using a LabRAM HR Horiba-Jobin Yvon spectrometer with a 532 nm excitation laser under ambient conditions. Low laser power (<1 mW) was used to avoid heat-induced modification or degradation of the sample due to the focused laser light during the spectrum acquisition. The collection time was larger than 200 s. The excitation laser beam was focused through a 50× optical microscope (spot size ∼1 mm and work distance 1 cm). The spectral resolution was ∼1 cm^{-1}.

3. RESULTS AND DISCUSSION

3.1. Scanning Electron Microscopy of Ln^{3+}/SF Samples. Figure 3 shows the previously acquired SEM images of Ln^{3+}/SF samples, compared with the natural silk cocoon and degummed SF.[23] All of the samples of regenerated lanthanide-doped SF fibers show a micro- and nanoscopic fibrous texture. In particular Ce/SF, Pr/SF, Er/SF, Tm/SF, Yb/SF, and Lu/SF exhibit a typical hemicylindrical cross section, with higher fiber diameters compared to undoped degummed SF. Lu/SF shows fiber dimensions similar to the degummed fibers; La/SF and Dy/SF, although macroscopically appear as fibrous threads, are actually composed of small, fragmented, and coarse fibers with irregular dimensions and structures.

3.2. Raman Spectroscopy of Ln^{3+}/SF Samples. Figure 4 shows Raman spectra of different lanthanide (Ln)-doped silk fibroin fibers, SF−Ln, (blue lines) with the spectrum of degummed silk fibroin, SF (red line), hydrated lanthanum(III)

https://doi.org/10.1021/acsomega.2c07149
ACS Omega 2023, 8, 24165−24175

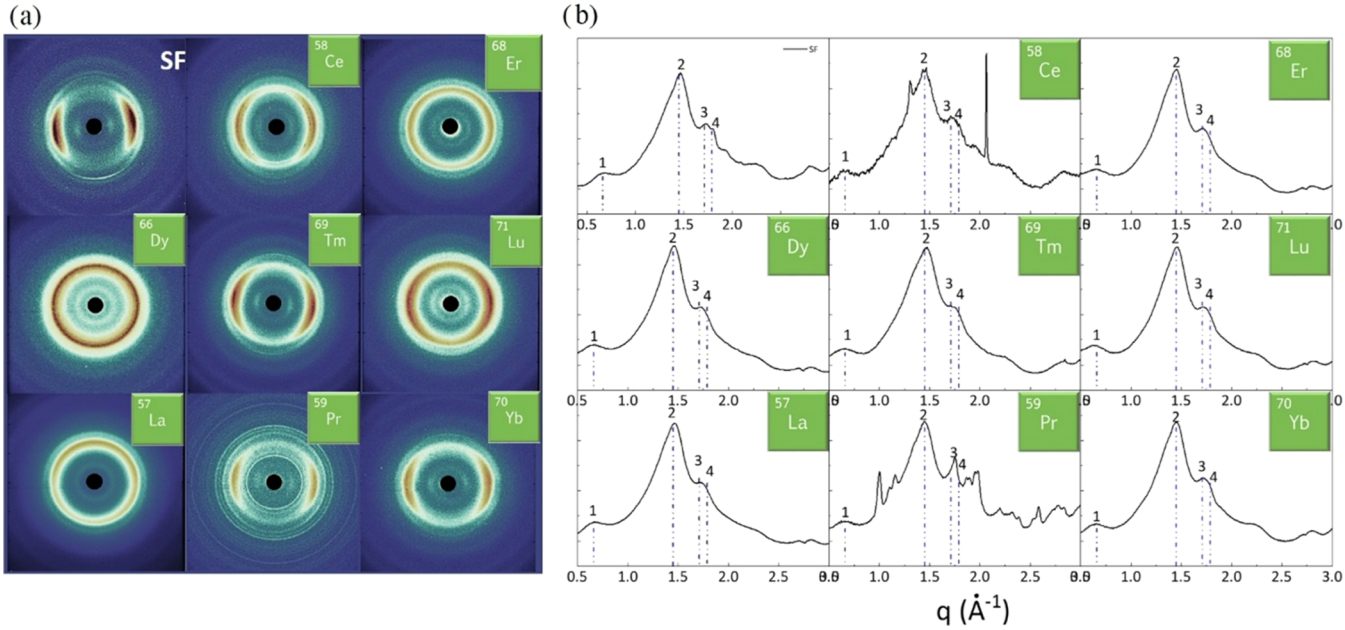

Figure 5. (a) 2D WAXS patterns of (A) degummed SF and regenerated fibers obtained after treatment with Ln^{3+}. (b) 1D WAXS profiles; vertical bars highlight the equatorial reflections at $q_1 = 0.66 \pm 0.075$ Å^{-1} ($d_1 = 9.5 \pm 1$ Å), $q_2 = 1.5 \pm 0.1$ Å−1 ($d_2 = 4.2 \pm 0.3$ Å), and $q_3 = 1.7 \pm 0.1$ Å^{-1} ($d_3 = 3.7 \pm 0.3$ Å) and the meridional reflection at $q_4 = 1.8 \pm 0.1$ Å^{-1} ($d_4 = 3.5 \pm 0.2$ Å). The equatorial and meridional peaks were indexed as follows: q_1 the (010) reflection; q_2 an overlap of the (020) and (210) reflections; and q_3 the (021) reflection.

trichloride, $LnCl_3$, and salts (black line) used to dope SF, in the energy range of 100−700 cm^{-1}, where Ln are La, Pr, Er, Dy, Ce, Lu, Tm, and Yb.

Spectra of all hydrated $LnCl_3$ salts show, in the range 100−700 cm^{-1}, characteristic vibrational bands due to the bond between lanthanide and oxygen, Ln−O, in particular at 112−113 cm^{-1} (known as E_g mode), 114−123 cm^{-1} (B_{1g} mode), 148−159 cm^{-1} (E_g mode), 226−252 cm^{-1} (E_g mode), 260−263 cm^{-1} (B_{1g} and B_{2g} modes), 374−382 cm^{-1} (A_{1g} mode), 458−494 cm^{-1} (B_{1g} mode), 520−565 cm$_{-1}$ (A_{1g} mode), and at 558−612 cm^{-1},[33−38] and bands due to the bond between lanthanide and nitrogen, Ln−N, in the range 406−470 cm^{-1}.[39] The Ln−O and Ln−N vibrational frequencies slightly change depending on the Ln ion because they are correlated with the Ln−O bond length.[40] The Raman spectrum of degummed SF (red line) shows broad bands at ∼230, 280, and 590 cm^{-1} due to the skeletal bending vibrations (C−C−C) and more intense bands at ∼350, 400, and 480 cm^{-1} due to the backbone deformation (C−C−C, C−C−N) in the range of 100−700 cm^{-1}.[41] After Ln doping, the Raman spectrum of pure SF strongly changes showing the presence of some additional broad bands (indicated in Figure 4 by *) that can be attributed to the formation of Ln−N and Ln−O bonds in SF. On analyzing, as an example, the evolution of the Raman spectrum of degummed SF before and after La doping, we found that the Raman spectrum of SF−La shows the presence of new peaks at ∼115, ∼130, ∼504, and ∼680 cm^{-1} that are not present before doping and are indicative of the formation of bonds between La and O in the SF. Moreover, it is interesting to highlight that, starting from the spectrum of pure degummed SF, the following changes can be noted upon doping: (i) the band at ∼230 cm^{-1} becomes more intense with a small blue shift after doping due to the contribution of the La−O bonds, (ii) the band at 350 cm^{-1} increases in intensity and slightly red-shifts due to the formation of La−O bonds, (iii) the band at 400 cm^{-1} blue-shifts and becomes more intense due to the contribution of the La−N band, (iv) the more intense peak at 480 cm^{-1} changes from a symmetric to an asymmetric shape and a shoulder at ∼504 cm^{-1} appears due to the blue-shifted contribution of the La−O band (strongly evident in the spectra of SF−La and SF−Pr), and finally (v) the band at 590 cm^{-1} strongly increases in intensity and red-shifts after doping. These changes are highlighted in Figure 4 by blue arrows in the spectrum of La−SF. All Ln-doped SFs show similar evolution in the Raman spectrum after doping and differences in the broadening and intensity of the additional bands after the formation of Ln−O and Ln−N bonds in Ln−SF, which are due to the different chemical nature of the Ln metal ions to the different doping quantities and to the high fluorescence of the SF that can cover weak Raman bands.

3.3. Solid-State Structure of Ln^{3+}/SF by WAXS. WAXS experiments were performed on the fibers obtained by Ce^{3+}, La^{3+}, Dy^{3+}, Er^{3+}, Tm^{3+}, Yb^{3+}, Lu^{3+}, and Pr^{3+} dissolution and fiber regeneration. The two-dimensional (2D) WAXS patterns, collected in the same explored volume (circular beam size at the sample was around 200 μm), once centered, calibrated, and folded into one-dimensional (1D) profiles (after integration along the entire azimuth), were compared with the WAXS patterns of the degummed SF,[22,23] and are reported in Figure 5 panel (a) and panel (b), respectively. Degummed SF exhibits the typical cross β-diffraction signal whose intensity is anisotropically distributed along two main orthogonal directions labeled as meridional, along the fiber axis, and equatorial, perpendicular to the fiber axis. It is well known that there are two kinds of crystalline forms, Silk I and Silk II for *B. mori* SF.[42] It is also overall recognized that the latter is the predominant structure after spinning in the solid state.[43,44] The 2D/1D data were univocally indexed as the fiber diffraction pattern of the *B. mori* Silk II structure,[45,46] which has an orthorhombic structure with unit cell dimensions $a = 9.68 \pm 0.20$ Å, $b = 9.36 \pm 0.18$ Å, and $c = 7.02 \pm 0.14$ Å. The equatorial peaks at $q_1 = 0.66 \pm 0.075$ Å^{-1} ($d_1 = 9.5 \pm 1$ Å), q_2

https://doi.org/10.1021/acsomega.2c07149
ACS Omega 2023, 8, 24165−24175

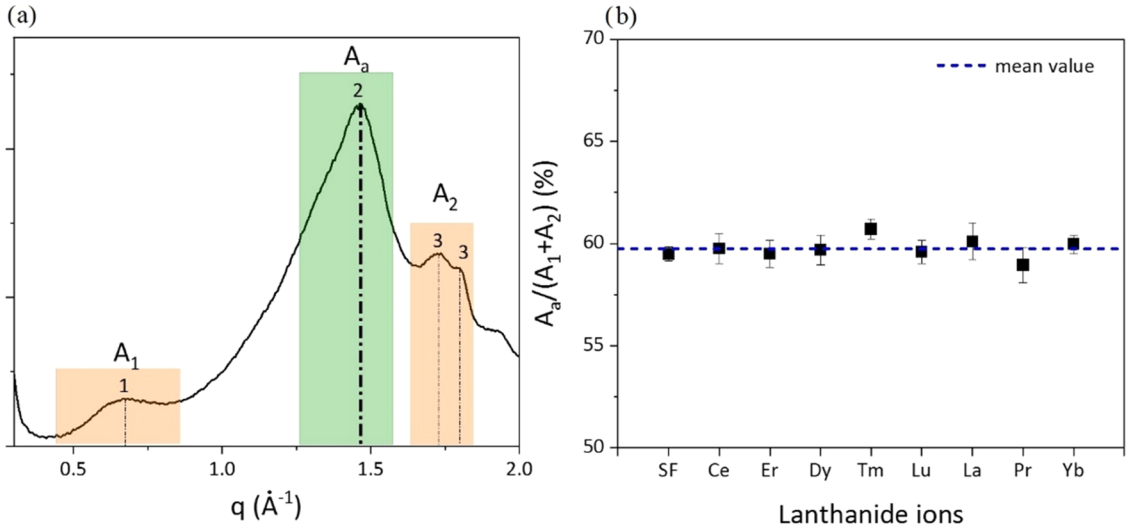

Figure 6. (a) Integral area and (b) amorphous/crystalline ratio vs lanthanide ions.

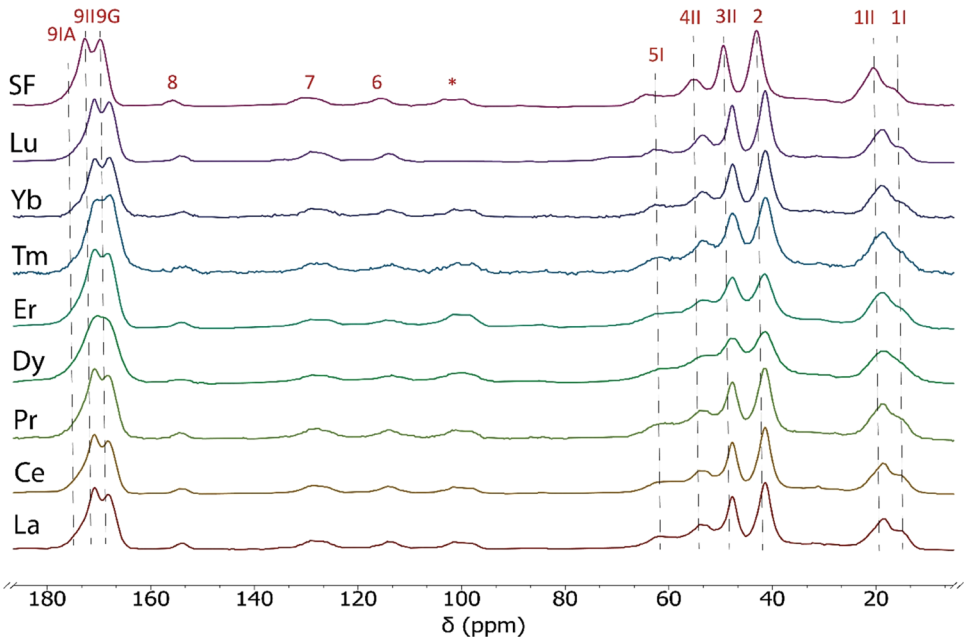

Figure 7. $^{1}H-^{13}C$ CPMAS spectra of degummed SF and of SF samples regenerated using the lanthanide salts $LnCl_3 \cdot xH_2O$ (Ln = La, Ce, Pr, Dy, Er, Tm, Yb, Lu; x = 6, 7). Spinning sidebands are marked with an asterisk. Vertical dashed lines indicate the position of the peaks labeled on the top of the figure according to Table 1. T = 298 K and spin rate = 7.0 kHz.

= 1.5 ± 0.1 Å^{-1} (d_2 = 4.3 ± 0.3 Å), and q_3 = 1.7 ± 0.1 Å^{-1} (d_3 = 3.7 ± 0.3 Å) were indexed as the (010), the overlap of the (020) and (210) reflections, and the (021) reflection, respectively. The meridional peak at q_4 = 1.8 ± 0.1 Å^{-1} (d_4 = 3.5 ± 0.2 Å), indexed as the (002) reflection, indicates the β-strands' distance along the fiber axis, which yields the c = 7.0 Å axial repetition and contains two peptide units.

Precisely, 2D WAXS data show that (i) fibers treated with Ce^{3+}, Tm^{3+}, Yb^{3+}, Lu^{3+}, and Pr^{3+} exhibit a 2D typical cross β-diffraction pattern, similar to that of the degummed SF, thus indicating a partial recovery of their fibrillar nature after reprecipitation. (ii) Fibers treated with La^{3+}, Dy^{3+}, and Er^{3+} show full diffraction rings, without any preferential orientation (Figure 5).

In fibers, the crystalline domains are embedded in a continuous matrix of amorphous material.[47] We used the WAXS data to determine the relative weight of these two components by the following procedure:

- For each 1D WAXS profile, the background was interpolated and subtracted.
- The relative weight of the amorphous to the crystalline phases was calculated by the ratio (Figure 6a):

$$A_a/(A_1 + A_2) \quad (1)$$

between the areas A_a in the range Δq = 1.15−1.61 Å^{-1} (amorphous), A_1 in the range Δq = 0.45−0.8 Å^{-1}, and A_2 in the q range Δq = 1.65−1.85 Å^{-1} (crystalline).
- The ratio obtained by eq 1 was reported in Figure 6b for each lanthanide ion.

In particular, samples treated with Ce^{3+}, Tm^{3+}, Yb^{3+}, Lu^{3+}, and Pr^{3+} exhibit a typical cross β-diffraction pattern analogue

https://doi.org/10.1021/acsomega.2c07149
ACS Omega 2023, 8, 24165−24175

to that of degummed SF, suggesting an almost complete recovery of crystallinity after the dialysis procedure.[22,23] On the contrary, La^{3+}, Dy^{3+}, and Er^{3+} gave a poorly oriented protein structure, with a diffraction pattern similar to raw silk in cocoons preliminary to sericin removal through boiling in basic aqueous solutions. Indeed, these samples have no preferential orientation, suggesting a fiber regenerating procedure with poor hierarchical order. Our analysis shows that the ratio between the amorphous and crystalline regions, reported in Figure 6b, does not show any significant variation among the investigated samples. In fact, the mean of the value obtained by eq 1 is about 60%, independently from the lanthanide used in the dissolution and regeneration of the SF fibers.

3.4. Structure of Ln^{3+}/SF by Solid-State NMR. Solid-state NMR is a well-established analytical tool to investigate SF conformations, thus enabling to correlate the protein secondary structures to processing and environmental conditions.[48−50] In particular, the ^{13}C NMR chemical shift in the solid state has long been exploited as an intrinsic probe to examine the conformation behavior of SF, taking advantage of the fact that the polymorphic structure of the samples in solid-state NMR analysis is fully preserved and that, differently from X-ray diffraction techniques, solid-state NMR analysis is suitable also for poorly crystalline materials. In this context, the shape of the signals can give information on the relative amount of the soluble helices/coil dominated structure, herein referred to as Silk I like, as proposed by Callone et al.,[51] with respect to the β-sheet/β-sheet-like crystal structure (herein referred to as Silk II like) in the regenerated samples.[47,52]

Moreover, the sharpness of the signals has been correlated to the degree of crystallinity, interaction with adsorbed water, or lateral chain mobility.[51]

The $^{1}H-^{13}C$ CPMAS spectra of the eight samples recovered after regeneration of the SF by Ajsawa's method using the lanthanide salts $LnCl_3 \cdot xH_2O$ (Ln = La, Ce, Pr, Dy, Er, Tm, Yb, Lu; x = 6, 7) as the chaotropic agents are shown in Figure 7 along with the spectrum of the degummed SF. The assignments of the signals, which are labeled from **1** to **9**, are reported in Table 1. When the assignment was unequivocal, the indication "I" or "II" was put aside the number identifying the peak to specify the contribution of Silk I like (I) or Silk II (II) configuration. It is apparent from Figure 7 that the spectra of the eight samples regenerated with lanthanide are similar to each other and only slightly highfield shifted (−2 ppm ca) with respect to that of degummed SF.

Table 1. ^{13}C Chemical Shifts of Main Components in SF Regenerated Using Lanthanide Ions as Chaotropic Agents[53−58a]

δ (ppm)		^{13}C labeling	component
15.1	C_β	**1-I**	Ala
21.1	C_β	**1-II**	Ala
41.4	C_α	**2**	Gly
47.8	C_α	**3-II**	Ala
50.1	C_α	**3-I**	Ala
53.4	C_α	**4-II**	Ser (+Tyr)
58.0	C_α	**4-I**	Ser
60.7	C_β	**5-I**	Ser
63.9	C_β	**5-II**	Ser
114.2	C_ε	**6**	Tyr
129.7	C_γ/C_δ	**7**	Tyr
154.2	C_ζ	**8**	Tyr
167.8	C=O	**9-G**	Gly
170.8	C=O	**9-IIA**	Ala
173.5	C=O	**9-IA**	Ala

[a]IA refers to the alanine signal in Silk I-like, IIA refers to the alanine signal in Silk II, and G refers to the glycine signal.

The peak centered at ca δ 18 ppm (signal **1**) is the convolution of four contributions: δ 15.0 ± 0.5 ppm (helix-like conformation), δ 17.0 ± 0.5 ppm (helix/random coil conformation), δ 20.0 ± 0.5 ppm (β-sheet conformation), and δ 21.5 ± 0.5 ppm (β-sheet-like conformation).[49,51,55,59−61] The profile fittings of signal **1**, carried out with MestReNova 11.0 software, gives the relative amount of the four contributions (Table S1), which are reported, for each sample, in Figure 8. Figure 9a shows the profile fittings of signal **1** for the sample "Ce" regenerated with $CeCl_3 \cdot 7H_2O$, while the profile fittings of signal **1** for all other samples are shown in Figure S1.

It is apparent from Figure 8 that in all samples, the predominant configuration is a β-sheet/β-sheet-like crystal structure (Silk II), in agreement with WAXS analysis. Taking degummed SF as a reference (whose content of Silk II is 84.1%), an increase of Silk I-like contribution was registered for samples treated with La^{3+} Ce^{3+}, Pr^{3+}, Dy^{3+}, Er^{3+}, and Tm^{3+}, while a slight decrease of Silk I-like contribution was observed for samples treated with Yb^{3+} and Lu^{3+}. This result suggests that the type of lanthanide used as the chaotropic agent influences, albeit to a little extent, the secondary structure of the regenerated SF.

The goodness of the profile fittings made with the four components at δ 15.0 ± 0.5, δ 17.0 ± 0.5, δ 20.0 ± 0.5, and δ 21.5 ± 0.5 ppm for all spectra in Figure 9 indicates that a possible contribution of 3_{10}-helix conformation (which would provide an additional peak centered at ca 18.2 ppm) is negligible in our samples.[51]

Figure 9b shows the $^{1}H-^{15}N$ CPMAS spectrum of the sample regenerated with Lu^{3+}, while the $^{1}H-^{15}N$ CPMAS spectra for all other samples are shown in Figure S2. The $^{1}H-^{15}N$ CPMAS spectrum can be subdivided into three parts: starting from low fields, the broad peak centered at δ 125 ppm is ascribed to alanine residues in Silk I-like and Silk II conformations; the shoulder at δ 121 ppm is ascribed to serine residues in Silk I-like and Silk II conformations overlapped with alanine residues in Silk I-like conformation; and the broad peak centered at δ 111 ppm is ascribed to glycine residues in Silk I-like and Silk II conformations.[62]

No significant difference is observed between the $^{1}H-^{15}N$ CPMAS spectra of the various SF samples discussed in this paper.

Inspection of Figure 7 reveals a profound difference in signal sharpness, which is best appreciated by focusing on signal **2**. Measuring the full width at half height (FWHH) of peak **2** for all silk samples (Table 2), it can be noted that Lu, La, Pr, Ce, and Yb displayed an FWHH ranging from 235 to 315 Hz, comparable to that of SF (278 Hz), while Tm, Er, and Dy displayed FWHHs of 400, 450, and 550 Hz, respectively. As mentioned above, the FWHH has been related to the crystallinity or lateral chain mobility in SF samples.[51] However, given that the linewidth of an NMR signal is related to the relaxation rate according to FWHH = $\frac{1}{\pi T_2}$ (where T_2 is the spin−spin relaxation time) and given that all lanthanide ions are paramagnetic, the question arises whether the different

https://doi.org/10.1021/acsomega.2c07149
ACS Omega 2023, 8, 24165−24175

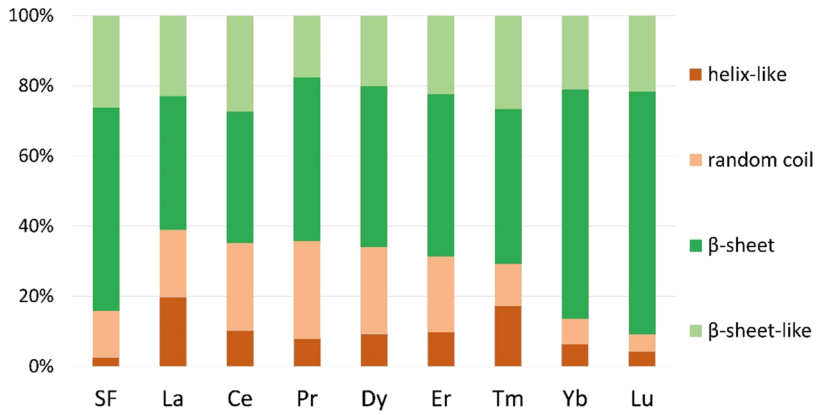

Figure 8. Relative contributions of helix-like (brown), helix/random coil (pink), β-sheet (dark green), and β-sheet-like (light green) conformations to the area of peak **1** in degummed (SF) and in SF samples regenerated using the lanthanide salts $LnCl_3{\cdot}xH_2O$ (Ln = La, Ce, Pr, Dy, Er, Tm, Yb, Lu; x = 6, 7).

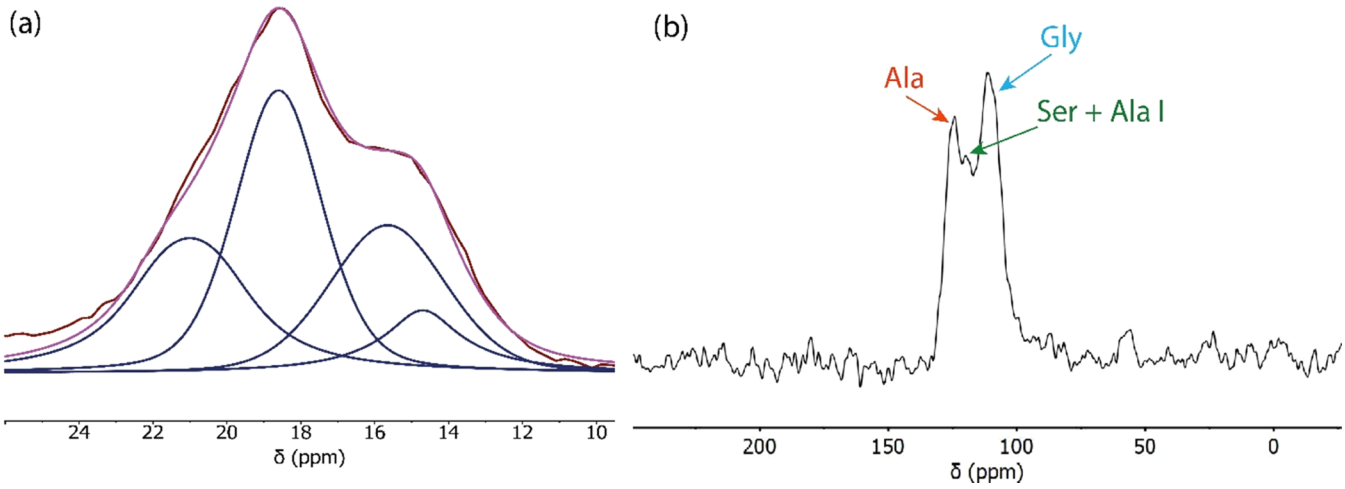

Figure 9. (a) Profile fitting of peak **1** from the $^1H-^{13}C$ CPMAS spectrum of SF samples regenerated using $CeCl_3{\cdot}7H_2O$. (b) $^1H-^{15}N$ CPMAS spectrum of the SF samples regenerated using $LuCl_3{\cdot}6H_2O$. T = 298 K and spin rate = 10.0 kHz.

Table 2. FWHH of Peak 2 and Magnetic Susceptivity of Lanthanide Ions Used as Chaotropic Agents

FWHH of peak **2** (Hz)	magnetic susceptivity $\chi_{mol}/10^{-3}$ ($cm^3{\cdot}mol^{-1}$)	lanthanide
550	98	Dy
450	48	Er
300	2.5	Ce
400	24.7	Tm
235	0.183	Lu
300	0.096	La
315	5.53	Pr
280	0.067	Yb

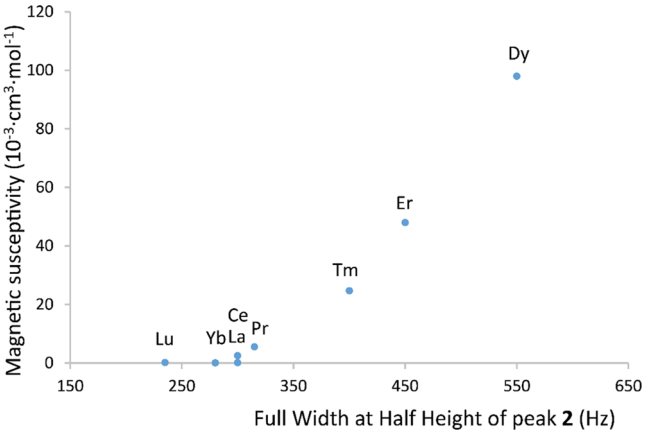

Figure 10. Correlation between the FWHH of peak **2** and the magnetic susceptivity of the lanthanide ion used as a chaotropic agent in the regeneration of SF.

broadness of the spectra shown in Figure 7 is to be attributed to the different degrees of crystallinity or to the paramagnetic effects due to lanthanide impurities in the sample. Figure 10 shows that there is a correlation between the FWHH of peak **2** and the magnetic susceptivity of the lanthanide ion used. This suggests that the paramagnetic effects due to lanthanide impurities may play a crucial role in signal sharpness. In order to check this hypothesis, we compared the crystallinity degree of the various samples determined by WAXS analysis, which pointed out that there is no significant influence from the lanthanide ion content on the amorphous/crystalline ratio that remains almost constant. This allows concluding that the signal sharpness is almost quantitatively determined by the different paramagnetic effects of all lanthanides involved in the dissolution and regeneration process of SF.

https://doi.org/10.1021/acsomega.2c07149
ACS Omega 2023, 8, 24165−24175

Comparison of the above-mentioned techniques is of fundamental importance when a new material must be fully characterized. In this study, Ln/SF samples were analyzed and compared by means of a complete understanding of assembly and structural features. Raman spectroscopy confirmed the doping effect of each lanthanide, also suggesting a direct coordinating ability of SF toward the metal ions via O−Ln and N−Ln bonds. SEM images gave information about the macroscopic appearance of all samples. Results are in agreement with the crystalline behavior of each sample through WAXS and SS-NMR techniques. La/SF and Dy/SF revealed a coarse and fragmented fiber structure, and WAXS analysis confirmed the low-ordered and poorly crystalline matter of the fibers treated with La^{3+} and Dy^{3+}. Er/SF gave instead a more regular and less fragmented fiber dispersion by SEM analyses, but still lacking crystallinity as confirmed by WAXS. Also, SS-NMR showed an increase of noncrystalline regions imputable to Silk I-like contributions for La/SF, Dy/SF, and Er/SF, together with Ce/SF, Pr/SF, and Tm/SF.

4. CONCLUSIONS

In this study, Ln−SF fibers, obtained by dissolution of degummed SF with hydrated lanthanide chlorides in a hydroalcoholic solution and subsequent dialysis, were studied by Raman, WAXS, and SS-NMR techniques. Raman spectroscopy demonstrated the presence of all lanthanide ions coordinated with the SF structure, mainly by direct metal−oxygen and metal−nitrogen bonds. WAXS confirmed the crystallinity of all of the samples, with similar crystalline content of Silk II structures independently from the Ln used, albeit only Ce^{3+}, Tm^{3+}, Yb^{3+}, Lu^{3+}, and Pr^{3+} showed a 2D diffraction pattern typical of degummed SF. SS-NMR spectroscopy, in agreement with WAXS, also showed that Ln−SF samples exhibited the β-sheet/β-sheet-like crystal structure ascribable to Silk II. Moreover, even if to a lesser extent, Silk I-like contribution variations were evident for samples, showing an increase for La^{3+} Ce^{3+}, Pr^{3+}, Dy^{3+}, Er^{3+}, and Tm^{3+} and a decrease for Yb^{3+} and Lu^{3+}. Comparison with WAXS was fundamental to explain the different sharpnesses of crystallinity detection peaks in SS-NMR, attributed to the paramagnetic behavior of the lanthanides present in the SF matrix.

■ ASSOCIATED CONTENT

Supporting Information

The Supporting Information is available free of charge at https://pubs.acs.org/doi/10.1021/acsomega.2c07149.

For further insights into the SS-NMR of each sample analyzed, an associated file is given, where collected SS-NMR deconvolution of $^{1}H-^{13}C$ CPMAS peaks at ca δ 18 ppm and SS-NMR $^{1}H-^{15}N$ CPMAS spectra of all of the Ln^{3+}/SF samples as well as the table collecting relative amounts of helix-like, helix/random coil, β-sheet, and β-sheet-like conformations from peak **1** profile fitting are given (PDF)

■ AUTHOR INFORMATION

Corresponding Authors

Cinzia Giannini − *CNR IC−Institute of Crystallography, Bari 70126, Italy;* orcid.org/0000-0003-0983-2885; Email: cinzia.giannini@ic.cnr.it

Piero Mastrorilli − *DICATECh, Politecnico di Bari, 70125 Bari, Italy*; Email: p.mastrorilli@poliba.it

Gianluca M. Farinola − *Dipartimento di Chimica, Università degli Studi di Bari Aldo Moro, 70125 Bari, Italy; Silklab, Department of Biomedical Engineering, Tufts University, Medford, Massachusetts 02155, United States;* orcid.org/0000-0002-1601-2810; Email: gianlucamaria.farinola@uniba.it

Authors

Giorgio Rizzo − *Dipartimento di Chimica, Università degli Studi di Bari Aldo Moro, 70125 Bari, Italy;* orcid.org/0000-0003-1734-9965

Valentina Petrelli − *DICATECh, Politecnico di Bari, 70125 Bari, Italy*

Teresa Sibillano − *CNR IC−Institute of Crystallography, Bari 70126, Italy*

Liberato De Caro − *CNR IC−Institute of Crystallography, Bari 70126, Italy*

Maria Michela Giangregorio − *Institute of Nanotechnology, CNR NANOTEC, c/o, Dipartimento di Chimica, Università di Bari, 70126 Bari, Italy*

Marco Lo Presti − *Silklab, Department of Biomedical Engineering, Tufts University, Medford, Massachusetts 02155, United States*

Fiorenzo G. Omenetto − *Silklab, Department of Biomedical Engineering, Tufts University, Medford, Massachusetts 02155, United States;* orcid.org/0000-0002-0327-853X

Complete contact information is available at: https://pubs.acs.org/10.1021/acsomega.2c07149

Author Contributions

This manuscript was written through the contributions of all authors. All authors have given approval to the final version of the manuscript.

Notes

The authors declare no competing financial interest.

■ ACKNOWLEDGMENTS

Dott. Emanuela Callone is gratefully acknowledged for helpful discussions on Solid-state NMR data analyses. Dario Lo Presti is acknowledged for graphical support. Rocco Lassandro is acknowledged for his support in the XMI-Lab at CNR-IC. This research was partially funded by the Extended Partnership PE00000004 "Made in Italy Circolare e Sostenibile" (MICS) project, funded by the European Union-Next Generation EU.

■ ABBREVIATIONS

SF, silk fibroin; WAXS, wide-angle X-ray scattering; SS-NMR, solid-state nuclear magnetic resonance; SEM, scanning electron microscopy; HF, heavy fibroin; LF, light fibroin; P-25, fibrohexamerin; HFIP, hexafluoroisopropanol; HFA, hexafluoroacetone; NMMO, *N*-methylmorpholine *N*-oxide; CPMAS, cross-polarization/magic angle spinning; FWHH, full width at half height

■ REFERENCES

(1) Hillyard, P. *The Private Life of Spiders*, 2nd ed.; New Holland Publishers, 2011.

(2) Craig, C. L. Evolution of Arthropod Silks. *Annu. Rev. Entomol.* **1997**, *42*, 231−267.

(3) Cebe, P.; Partlow, B. P.; Kaplan, D. L.; Wurm, A.; Zhuravlev, E.; Schick, C. Silk I and Silk II Studied by Fast Scanning Calorimetry. *Acta Biomater.* **2017**, *55*, 323−332.

(4) Qi, Y.; Wang, H.; Wei, K.; Yang, Y.; Zheng, R. Y.; Kim, I. S.; Zhang, K. Q. A Review of Structure Construction of Silk Fibroin Biomaterials from Single Structures to Multi-Level Structures. *Int. J. Mol. Sci.* **2017**, *18*, No. 237.
(5) Koh, L. D.; Cheng, Y.; Teng, C. P.; Khin, Y. W.; Loh, X. J.; Tee, S. Y.; Low, M.; Ye, E.; Yu, H. D.; Zhang, Y. W.; Han, M. Y. Structures, Mechanical Properties and Applications of Silk Fibroin Materials. *Prog. Polym. Sci.* **2015**, *46*, 86−110.
(6) Zhou, C.-Z. Fine Organization of *Bombyx mori* Fibroin Heavy Chain Gene. *Nucleic Acids Res.* **2000**, *28*, 2413−2419.
(7) Inoue, S.; Tanaka, K.; Arisaka, F.; Kimura, S.; Ohtomo, K.; Mizuno, S. Silk Fibroin of *Bombyx mori* Is Secreted, Assembling a High Molecular Mass Elementary Unit Consisting of H-Chain, L-Chain, and P25, with a 6:6:1 Molar Ratio. *J. Biol. Chem.* **2000**, *275*, 40517−40528.
(8) Long, D.; Lu, W.; Zhang, Y.; Guo, Q.; Xiang, Z.; Zhao, A. New Insight into the Mechanism Underlying Fibroin Secretion in Silkworm, *Bombyx mori*. *FEBS J.* **2015**, *282*, 89−101.
(9) Murphy, A. R.; Kaplan, D. L. Biomedical Applications of Chemically-Modified Silk Fibroin. *J. Mater. Chem.* **2009**, *19*, 6443−6450.
(10) Wang, Q.; Chen, Q.; Yang, Y.; Shao, Z. Effect of Various Dissolution Systems on the Molecular Weight of Regenerated Silk Fibroin. *Biomacromolecules* **2013**, *14*, 285−289.
(11) Um, I. C.; Kweon, H. Y.; Park, Y. H.; Hudson, S. Structural Characteristics and Properties of the Regenerated Silk Fibroin Prepared from Formic Acid. *Int. J. Biol. Macromol.* **2001**, *29*, 91−97.
(12) Hess, S.; Van Beek, J.; Pannell, L. K. Acid Hydrolysis of Silk Fibroins and Determination of the Enrichment of Isotopically Labeled Amino Acids Using Precolumn Derivatization and High-Performance Liquid Chromatography-Electrospray Ionization-Mass Spectrometry. *Anal. Biochem.* **2002**, *311*, 19−26.
(13) Lorimer, R.; Arbor, A. *HYDROLYSIS Silk Peptones* 1934, 667 673.
(14) Ki, C. S.; Lee, K. H.; Baek, D. H.; Hattori, M.; Um, I. C.; Ihm, D. W.; Park, Y. H. Dissolution and Wet Spinning of Silk Fibroin Using Phosphoric Acid/Formic Acid Mixture Solvent System. *J. Appl. Polym. Sci.* **2007**, *105*, 1605−1610.
(15) Rockwood, D. N.; Preda, R. C.; Yücel, T.; Wang, X.; Lovett, M. L.; Kaplan, D. L. Materials Fabrication from *Bombyx mori* Silk Fibroin. *Nat. Protoc.* **2011**, *6*, 1612−1631.
(16) Ajisawa, A. Dissolution Aqueous of Silk Fibroin with Calciumchloride / Ethanol Solution. *J. Seric. Sci. Jpn.* **1997**, *67*, 91−94.
(17) Ha, S.-W.; Park, Y. H.; Hudson, S. M. Dissolution of Bombyx m Ori Silk Fibroin in the Calcium Nitrate Tetrahydrate−Methanol System and Aspects of Wet Spinning of Fibroin Solution. *Biomacromolecules* **2003**, *4*, 488−496.
(18) Kauffman, G. B. Profiles in Chemistry: Eduard Schweizer (1818−1860): The Unknown Chemist and His Well-Known Reagent. *J. Chem. Educ.* **1984**, *61*, No. 1095.
(19) Yoshioka, T.; Tashiro, K.; Ohta, N. Molecular Orientation Enhancement of Silk by the Hot-Stretching-Induced Transition from α-Helix-HFIP Complex to β-Sheet. *Biomacromolecules* **2016**, *17*, 1437−1448.
(20) Moseti, K. O.; Yoshioka, T.; Kameda, T.; Nakazawa, Y. Structure Water-Solubility Relationship in α-Helix-Rich Films Cast from Aqueous and 1,1,1,3,3,3-Hexafluoro-2-Propanol Solutions of S. c. Ricini Silk Fibroin. *Molecules* **2019**, *24*, No. 3945.
(21) Rosenau, T.; Potthast, A.; Adorjan, I.; Hofinger, A.; Sixta, H.; Firgo, H.; Kosma, P. Cellulose Solutions in N-Methylmorpholine-N-Oxide (NMMO) - Degradation Processes and Stabilizers. *Cellulose* **2002**, *9*, 283−291.
(22) Rizzo, G.; LoPresti, M.; Giannini, C.; Sibillano, T.; Milella, A.; Matzeu, G.; Musio, R.; Omenetto, F. G.; Farinola, G. M. Silk Fibroin Processing from CeCl3 Aqueous Solution: Fibers Regeneration and Doping with Ce(III). *Macromol. Chem. Phys.* **2020**, *221*, No. 2000066.
(23) Rizzo, G.; Lo Presti, M.; Giannini, C.; Sibillano, T.; Milella, A.; Guidetti, G.; Musio, R.; Omenetto, F. G.; Farinola, G. M. *Bombyx mori* Silk Fibroin Regeneration in Solution of Lanthanide Ions: A Systematic Investigation. *Front. Bioeng. Biotechnol.* **2021**, *9*, No. 653033.
(24) Rizzo, G.; Albano, G.; Lo Presti, M.; Milella, A.; Omenetto, F. G.; Farinola, G. M. Palladium Supported on Silk Fibroin for Suzuki−Miyaura Cross-Coupling Reactions. *Eur. J. Org. Chem.* **2020**, *2*, 6992−6996.
(25) Rizzo, G.; Albano, G.; Sibillano, T.; Giannini, C.; Musio, R.; Omenetto, F. G.; Farinola, G. M. Silk Fibroin-Supported Palladium Catalyst for Suzuki-Miyaura and Ullmann Coupling Reactions of Aryl Chlorides. *Eur. J. Org. Chem.* **2022**, *2022*, No. e202101567.
(26) Izumi, Y. Studies on the Silk-Palladium Catalyst. I Preparation and Stability. *Bull. Chem. Soc. Jpn.* **1959**, *32*, 932−936.
(27) Efficiency, C.; Compounds, V.. *Studies on the Silk Platinum Catalyst. Its Preparation and Activity By Akira AKAMATSU, Yoshiharu IZUMI and Shiro AKABORI* **1961**, *1067*, 1302−1306.
(28) Akamatsu, A.; Izumi, Y.; Akabori, S. Studies on the Silk-Rhodium Catalyst. *Bull. Chem. Soc. Jpn.* **1962**, *35*, 1706−1711.
(29) Rockwood, D. N.; Preda, R. C.; Yücel, T.; Wang, X.; Lovett, M. L.; Kaplan, D. L. MaterialsFabrication from *Bombyx mori* Silk Fibroin. *Nat. Protoc.* **2011**, *6*, 1612−1631.
(30) Altamura, D.; Lassandro, R.; Vittoria, F. A.; De Caro, L.; Siliqi, D.; Ladisa, M.; Giannini, C. X-Ray Microimaging Laboratory (XMI-LAB). *J. Appl. Crystallogr.* **2012**, *45*, 869−873.
(31) Sibillano, T.; De Caro, L.; Scattarella, F.; Scarcelli, G.; Siliqi, D.; Altamura, D.; Liebi, M.; Ladisa, M.; Bunk, O.; Giannini, C. Interfibrillar Packing of Bovine Cornea by Table-Top and Synchrotron Scanning SAXS Microscopy. *J. Appl. Crystallogr.* **2016**, *49*, 1231−1239.
(32) Siliqi, D.; De Caro, L.; Ladisa, M.; Scattarella, F.; Mazzone, A.; Altamura, D.; Sibillano, T.; Giannini, C. SUNBIM: A Package for X-Ray Imaging of Nano- and Biomaterials Using SAXS, WAXS, GISAXS and GIWAXS Techniques. *J. Appl. Crystallogr.* **2016**, *49*, 1107−1114.
(33) Santos, C. C.; Silva, E. N.; Ayala, A. P.; Guedes, I.; Pizani, P. S.; Loong, C.-K.; Boatner, L. A. Raman Investigations of Rare Earth Orthovanadates. *J. Appl. Phys.* **2007**, *101*, No. 053511.
(34) Wheeler, D. W.; Khan, I. A Raman Spectroscopy Study of Cerium Oxide in a Cerium−5wt.% Lanthanum Alloy. *Vib. Spectrosc.* **2014**, *70*, 200−206.
(35) Dogra, S.; Singh, J.; Sharma, N. D.; Samanta, K.; Poswal, H. K.; Sharma, S. M.; Bandyopadhyay, A. K. Phase Progression via Phonon Modes in Lanthanide Dioxides under Pressure. *Vib. Spectrosc.* **2014**, *70*, 193−199.
(36) Yu, J.; Cui, L.; He, H.; Yan, S.; Hu, Y.; Wu, H. Raman Spectra of RE2O3 (RE = Eu, Gd, Dy, Ho, Er, Tm, Yb, Lu, Sc and Y): Laser-Excited Luminescence and Trace Impurity Analysis. *J. Rare Earths* **2014**, *32*, 1−4.
(37) Riri, M.; Hor, M.; Serdaoui, F.; Hlaibi, M. Complexation of Trivalent Lanthanide Cations by Different Chelation Sites of Malic and Tartric Acid (Composition, Stability and Probable Structure). *Arabian J. Chem.* **2016**, *9*, S1478−S1486.
(38) Yan, D.; Wu, P.; Zhang, S. P.; Liang, L.; Yang, F.; Pei, Y. L.; Chen, S. Assignments of the Raman Modes of Monoclinic Erbium Oxide. *J. Appl. Phys.* **2013**, *114*, No. 193502.
(39) Kovács, A.; Apostolidis, C.; Walter, O.; Lindqvist-Reis, P. 'Lanthanide Contraction' in [Ln(BTP)3](CF3SO3)3 Complexes. *Struct. Chem.* **2015**, *26*, 1287−1295.
(40) Belova, N. V.; Sliznev, V. V.; Christen, D. Infrared and Raman Spectra of Tris(Dipivaloylmethanato) Lanthanides, Ln(Thd)3 (Ln = La, Nd, Eu, Gd, Tb, Ho, Er, Tm, Yb, Lu). *J. Mol. Struct.* **2017**, *1132*, 34−43.
(41) Xu, W.; Sun, Y.; Dong, X.; Li, S.; Wang, H.; Xue, J.; Zheng, X. Local Order and Vibrational Coupling of the C═O Stretching Mode of γ-Caprolactone in Liquid Binary Mixtures. *Sci. Rep.* **2017**, *7*, No. 12182.
(42) Lotz, B.; Cesari, F. C. The Chemical Structure and the Crystalline Structures of *Bombyx mori* Silk Fibroin. *Biochimie* **1979**, *61*, 205−214.

https://doi.org/10.1021/acsomega.2c07149
ACS Omega 2023, 8, 24165−24175

(43) Marsh, R. E.; Corey, R. B.; Pauling, L. An Investigation of the Structure of Silk Fibroin. *Biochim. Biophys. Acta* **1955**, *16*, 1−34.
(44) Asakura, T. Structure of Silk I (*Bombyx mori* Silk Fibroin before Spinning) -Type II β-Turn, Not α-Helix-. *Molecules* **2021**, *26*, No. 3706.
(45) Fossey, S. A.; Némethy, G.; Gibson, K. D.; Scheraga, H. A. Conformational Energy Studies of β-Sheets of Model Silk Fibroin Peptides. I. Sheets of Poly(Ala-Gly) Chains. *Biopolymers* **1991**, *31*, 1529−1541.
(46) Guo, C.; Zhang, J.; Jordan, J. S.; Wang, X.; Henning, R. W.; Yarger, J. L. Structural Comparison of Various Silkworm Silks: An Insight into the Structure-Property Relationship. *Biomacromolecules* **2018**, *19*, 906−917.
(47) Asakura, T.; Yao, J.; Yamane, T.; Umemura, K.; Ulrich, A. S. Heterogeneous Structure of Silk Fibers from Bombyx m Ori Resolved by 13 C Solid-State NMR Spectroscopy. *J. Am. Chem. Soc.* **2002**, *124*, 8794−8795.
(48) Ohgo, K.; Bagusat, F.; Asakura, T.; Scheler, U. Investigation of Structural Transition of Regenerated Silk Fibroin Aqueous Solution by Rheo-NMR Spectroscopy. *J. Am. Chem. Soc.* **2008**, *130*, 4182−4186.
(49) Asakura, T.; Suzuki, Y.; Nakazawa, Y.; Holland, G. P.; Yarger, J. L. Elucidating Silk Structure Using Solid-State NMR. *Soft Matter* **2013**, *9*, No. 11440.
(50) Asakura, T.; Aoki, A.; Komatsu, K.; Ito, C.; Suzuki, I.; Naito, A.; Kaji, H. Lamellar Structure in Alanine−Glycine Copolypeptides Studied by Solid-State NMR Spectroscopy: A Model for the Crystalline Domain of *Bombyx mori* Silk Fibroin in Silk II Form. *Biomacromolecules* **2020**, *21*, 3102−3111.
(51) Callone, E.; Dirè, S.; Hu, X.; Motta, A. Processing Influence on Molecular Assembling and Structural Conformations in Silk Fibroin: Elucidation by Solid-State NMR. *ACS Biomater. Sci. Eng.* **2016**, *2*, 758−767.
(52) Zhang, H.; Li, L.; Dai, F.; Zhang, H.; Ni, B.; Zhou, W.; Yang, X.; Wu, Y. Preparation and Characterization of Silk Fibroin as a Biomaterial with Potential for Drug Delivery. *J. Transl. Med.* **2012**, *10*, No. 117.
(53) Asakura, T.; Yao, J. 13C CP/MAS NMR Study on Structural Heterogeneity in *Bombyx mori* Silk Fiber and Their Generation by Stretching. *Protein Sci.* **2009**, *11*, 2706−2713.
(54) Saitô, H.; Tabeta, R.; Asakura, T.; Iwanaga, Y.; Shoji, A.; Ozaki, T.; Ando, I. High-Resolution 13C Nmr Study of Silk Fibroin in the Solid State by the Cross-Polarization-Magic Angle Spinning Method. Conformational Characterization Of Silk i and Silk Ii Type Forms of *Bombyx mori* Fibroin by the Conformation-Dependent 13C Chemical Shif. *Macromolecules* **1984**, *17*, 1405−1412.
(55) Asakura, T.; Watanabe, Y.; Uchida, A.; Minagawa, H. NMR of Silk Fibroin. Carbon-13 NMR Study of the Chain Dynamics and Solution Structure of *Bombyx mori* Silk Fibroin. *Macromolecules* **1984**, *17*, 1075−1081.
(56) Asakura, T.; Sugino, R.; Yao, J.; Takashima, H.; Kishore, R. Comparative Structure Analysis of Tyrosine and Valine Residues in Unprocessed Silk Fibroin (Silk I) and in the Processed Silk Fiber (Silk II) from *Bombyx mori* Using Solid-State 13 C, 15 N, and 2 H NMR. *Biochemistry* **2002**, *41*, 4415−4424.
(57) Zhou, P.; Li, G.; Shao, Z.; Pan, X.; Yu, T. Structure of *Bombyx mori* Silk Fibroin Based on the DFT Chemical Shift Calculation. *J. Phys. Chem. B* **2001**, *105*, 12469−12476.
(58) Sato, H.; Kizuka, M.; Nakazawa, Y.; Asakura, T. The Influence of Ser and Tyr Residues on the Structure of *Bombyx mori* Silk Fibroin Studied Using High-Resolution Solid-State 13C NMR Spectroscopy and 13C Selectively Labeled Model Peptides. *Polym. J.* **2008**, *40*, 184−185.
(59) Ji, D.; Deng, Y.; Bin; Zhou, P. Folding Process of Silk Fibroin Induced by Ferric and Ferrous Ions. *J. Mol. Struct.* **2009**, *938*, 305−310.
(60) Asakura, T.; Sato, H.; Moro, F.; Nakazawa, Y.; Aoki, A. Lamellar Structure in Poly(Ala-Gly) Determined by Solid-State NMR and Statistical Mechanical Calculations. *J. Am. Chem. Soc.* **2007**, *129*, 5703−5709.
(61) Santi, S.; Mancini, I.; Dirè, S.; Callone, E.; Speranza, G.; Pugno, N.; Migliaresi, C.; Motta, A. A Bio-Inspired Multifunctionalized Silk Fibroin. *ACS Biomater. Sci. Eng.* **2021**, *7*, 507−516.
(62) Asakura, T.; Demura, M.; Date, T.; Miyashita, N.; Ogawa, K.; Williamson, M. P. NMR Study of Silk I Structure of *Bombyx mori* Silk Fibroin with 15N- and 13C-NMR Chemical Shift Contour Plots. *Biopolymers* **1997**, 193−203.

https://doi.org/10.1021/acsomega.2c07149
ACS Omega 2023, 8, 24165−24175